Assessment of the relationship between magnetotransport and magnetocaloric properties in nano-sized La0.7Ca0.3Mn1-xNixO3 manganites

Article *in* Journal of Magnetism and Magnetic Materials · September 2018

DOI: 10.1016/j.jmmm.2018.09.036

CITATION
1

READS
159

7 authors, including:

Adrián Gómez
National University of Colombia
25 PUBLICATIONS **78** CITATIONS
SEE PROFILE

Edgar Chavarriaga
Universidad Católica Luis Amigó, Medellín, Colombia
26 PUBLICATIONS **40** CITATIONS
SEE PROFILE

Jesús Prado-Gonjal
Complutense University of Madrid
59 PUBLICATIONS **646** CITATIONS
SEE PROFILE

Nestor Rojas
National University of Colombia - Medellín
30 PUBLICATIONS **25** CITATIONS
SEE PROFILE

Journal of Magnetism and Magnetic Materials 469 (2019) 558–569

Contents lists available at ScienceDirect

Journal of Magnetism and Magnetic Materials

journal homepage: www.elsevier.com/locate/jmmm

Assessment of the relationship between magnetotransport and magnetocaloric properties in nano-sized $La_{0.7}Ca_{0.3}Mn_{1-x}Ni_xO_3$ manganites

A. Gómez[a], E. Chavarriaga[b], J.L. Izquierdo[a], J. Prado-Gonjal[c], F. Mompean[c], N. Rojas[d], O. Morán[b,*]

[a] Institución Universitaria Pascual Bravo, Centro de Investigación y Desarrollo en Materialografía, Calle 73 No. 73A-226, C.P. 050001 Medellín, Colombia
[b] Universidad Nacional de Colombia, sede Medellín, Facultad de Ciencias, Departamento de Física, Advanced Oxides Group, A.A. 568 Medellín, Colombia
[c] Instituto de Ciencia de Materiales de Madrid, CSIC, Sor Juana Inés de la Cruz s/n, 28049 Madrid, Spain
[d] Universidad Nacional de Colombia, sede Medellín, Facultad de Minas, Instituto de Minerales (CIMEX), A.A. 568 Medellín, Colombia

A B S T R A C T

The effect of Ni^{2+} substitution on the magneto-transport properties and the concomitant relationship with the magnetocaloric function of nano-sized $La_{0.7}Ca_{0.3}Mn_{1-x}Ni_xO_3$ (x = 0, 0.02, 0.07, and 0.10) perovskite manganites are reported. All the samples were synthesized using the auto-combustion method. X-ray diffraction analysis studies confirmed the phase purity of the synthesized samples. The substitution of Mn^{3+} ions with Ni^{2+} ions in the $La_{0.7}Ca_{0.3}MnO_3$ lattice was also verified using this technique. Rietveld analysis indicated that the volume of the unit cell increased with increasing Ni^{2+} content. Zero-field-cooled and field-cooled magnetization showed that all samples underwent a paramagnetic-ferromagnetic phase transition, which was concomitant with a metal-insulator transition. A small deviation between the zero-field-cooled and field-cooled magnetization curves was observed when the measurements were carried out in a field of 1000 Oe. The Curie temperature decreased systematically from 264 K for x = 0 to 174 K for x = 0.10. Probably the doping at the Mn^{3+} sites with Ni^{2+} ions in the $La_{0.7}Ca_{0.3}MnO_3$ lattice weakened the Mn^{3+}-O-Mn^{4+} double exchange interaction, which led to a decrease in the transition temperature. The metal-insulator transition also shifted to lower temperatures upon Ni^{2+} substitution, and the value of the resistivity increased. Different conduction mechanisms were found in different temperature regions. Important physical parameters such as the polaron activation energy were obtained from the fit of the models to the experimental data. Arrot's plots revealed a second-order nature of the magnetic transition for all the samples, which was also confirmed by Landau's theory and universal curves. The second-order character of the magnetic phase transition observed in the pristine $La_{0.7}Ca_{0.3}MnO_3$ sample may be attributed to effects of the downsizing of the particle. Interestingly, a notable increase in the value of the magnetic entropy change was observed at Ni^{2+} doping levels as low as 2%. The magnetoresistance underwent a great change near the magnetic transition temperature, suggesting a close relationship between the magnetocaloric effect and magnetotransport properties in $La_{0.7}Ca_{0.3}MnO_3$ manganites. Such behavior can be attributed to the spin order/disorder feature, which plays a crucial role in both effects. On the other hand, the value of the magnetoresistance of the pristine $La_{0.7}Ca_{0.3}MnO_3$ sample increased upon Ni^{2+} doping, which is probably related to the downsizing of the particles.

1. Introduction

Manganite materials with the composition $R_{1-x}A_xMnO_3$ (R = rare earth elements such as La, Nd, Pr, and Sm, and A = divalent alkaline elements such as Ca, Ba, and Sr) have received increasing attention due to their special properties, such as colossal magnetoresistance (CMR), metal–insulator (MI) transition, and the magnetocaloric effect (MCE) [1,2]. In particular, magnetic refrigeration, based on MCE, is considered to be an alternative to the well-established compression-evaporation cycle for room-temperature applications [3]. Apart from the manganites, a variety of materials that exhibit a large MCE have been studied, and the relevant results have been summarized in several review articles [4–6]. To mention just a few examples, Gd is among the pure lanthanide elements exhibiting MCE, the only pure metal with T_C close to room temperature [4]. Interestingly, room temperature MCE has been studied for other Gd-M binary compounds such as $Gd_{0.85}Y_{0.15}$, $Gd_{0.85}Tb_{0.15}$ [7], and $Gd_{0.75}Zn_{0.25}$ [8] systems. Composites of $Gd_{1-x}Ho_x$ alloys (x = 0, 0.09, 0.20) have recently been considered for optimizing the MCE response within the temperature range 265–293 K, which is desirable for the Ericsson refrigeration cycle [9]. Other interesting MCE materials are the AB_2 intermetallic compounds known as Laves phases [10]. In the AB_2 stoichiometry, A represents a rare-earth metal (including Sc and Y) and B mainly a transition metal. The transition temperatures of most of the Laves phases, which are attractive for MCE, lie below 100 K. Laves phases with transition temperatures above 100 K generally contain Co as a transition metal [11].

Other MCE materials that have recently been investigated are La$(Fe_{1-x}Si_x)_{13}$ alloys and their hydrides La$(Fe_{1-x}Si_x)_{13}H_y$, $MnFePxAs_{1-x}$ alloys, and $Ni_{2-x}Mn_{1-x}Ga$ Heusler alloys [12–15]. Although synthesis of these systems requires very controlled conditions, the achieved

* Corresponding author.
E-mail address: omoranc@unal.edu.co (O. Morán).

https://doi.org/10.1016/j.jmmm.2018.09.036
Received 16 May 2018; Received in revised form 8 August 2018; Accepted 7 September 2018
Available online 08 September 2018
0304-8853/

results show that they are potentially interesting for practical applications in magnetic refrigeration. Nevertheless, several disadvantages, such as large thermal and/or field hysteresis and high production costs, hamper the use of these materials in actual magnetic refrigerant applications. In this regard, perovskite-type manganites not only exhibit a large MCE but also high refrigeration efficiency, low-cost production, chemical stability, and a broad working temperature [16]. In addition, the manganites are environmentally friendly and nontoxic, and they do not cause noise pollution. These characteristics make them attractive for further research in refrigeration technology not based on gas compression.

Generally speaking, the large magnetic entropy change (ΔS_M) observed in perovskite manganites is mainly linked to the variation of the double exchange (DE) interaction of the Mn^{3+} and Mn^{4+} ions [17]. It has also been suggested that the strong spin-lattice coupling in the magnetic ordering process could also play an important role in the large magnetic entropy change in perovskite manganites [18]. The considerable lattice changes that accompany the magnetic transition in perovskite manganites indicate that there is a strong coupling between spin and lattice in this kind of material [19]. Concretely, the lattice structural change in the Mn–O bond distance and in the⟨Mn–O–Mn⟩ bond angle would favor spin ordering. As a consequence, a more abrupt variation of the magnetization near T_C will happen, leading to a large ΔS_M and therefore to a large MCE.

When the particle size is reduced to a few tens of nanometers, the properties of perovskite manganites are quite different from those at the microscale [20,21]. For instance, low saturation magnetization and low-field magnetoresistance (MR) are some special effects observed in nanometric manganites [22–25]. Recent reports have shown that the reduction of the particle size plays an important role in the determination of the change in magnetic entropy [26].

In recent years, the issue of replacing the Mn site with non-magnetic and magnetic ions has received special attention [27,28]. This is because Mn-site doping allows one to explore more information about the structural, magnetic, and transport properties of these complex materials. It has been argued that the study of doping effects at the Mn site by other elements with different electronic configurations and ionic radii, such as Fe, Co, Cr, and Ni, deserves particular emphasis because of the decisive role of Mn ions in the colossal magnetoresistance materials [29]. In particular, the substitution of Mn^{3+} with Ni^{2+} ions in the pristine LCMO lattice directly influences its magnetic and electrical properties [30]. Concretely, the replacement of Mn^{3+} with Ni^{2+} modifies the ratio of Mn^{3+}–O_2–Mn^{4+} bonds, which leads to a weakening of the DE interaction. Consequently, the transition temperature T_C is reduced and the resistivity increased. Likewise, the competition between FM and AFM exchange interactions is reinforced [31]. Indeed, Ni^{2+} substitution for Mn^{3+} increases the number of Mn^{4+} [32]. This in turn leads to an increase in the AFM interaction pairs such as Mn^{4+}–Mn^{4+}, Ni^{2+}–Mn^{3+}, and Ni^{2+}–Ni^{2+} [33]. Thus the magnetic interactions in the Ni^{2+}-doped LCMO samples are different from those of the undoped ones.

The influence of Ni^{2+} doping at the Mn site on the structural, magnetic, and MCE properties of CMR manganites has been reported in several papers [33–35]. Nevertheless, the greatest part of the results reported in these references was achieved on samples synthesized by conventional solid-state reaction, which produces grain sizes in the micrometer range. As previously stated, particle size plays an obvious role in the determination of the change in magnetic entropy and the magnetotransport properties of manganites [26]. In this connection, the standard solid-state reaction method is not appropriate for a variety of advanced applications, due to the formation of large particles, agglomerates, poor homogeneity, undesirable phases, irregular grain growth, lower reproducibility, and an imprecise stoichiometric control of cations [30]. Therefore, efficient processing methods based on wet chemistry should be tested in order to improve the homogeneity and reproducibility of perovskite-type materials [36].

In the present investigation, the auto-combustion method was successfully used to produce high-quality, nanometric $La_{0.7}Ca_{0.3}Mn_{1-x}Ni_xO_3$ samples. Compared to the standard solid-state reaction, this method has potential advantages, such as better homogeneities, lower processing temperatures, and short annealing times. Thus the auto-combustion method is a straightforward preparation process for producing homogeneous, very fine, crystalline, and unagglomerated multicomponent oxide powders without intermediate decomposition steps [36].

The aim of this paper is to study the effect of low Ni^{2+} doping levels on the magnetocaloric and magnetotransport properties of nanometric LCMO samples. The possibility of using a manganite that exhibits a second-order phase transition (SOPT) for refrigeration is evaluated by estimating the magnitude of the magnetocaloric effect and the relative cooling power. Furthermore, the relationship between the change in the resistivity and the magnetic entropy is explored.

2. Experiment

The synthesis of polycrystalline $La_{0.7}Ca_{0.3}Mn_{1-x}Ni_xO_3$ (x = 0, 0.02, 0.07, and 0.1) samples has been reported in a previous paper [37]. In short, the samples were synthesized via the combustion method with stoichiometric amounts of high-purity (99.99%, Sigma Aldrich) La $(NO_3)_3{\cdot}6H_2O$, $Ca(NO_3)_2{\cdot}4H_2O$, $Ni(NO_3)_2{\cdot}6H_2O$, and $Mn(C_2H_3O_2)_2{\cdot}4H_2O$ as starting reagents. Glycine was used as fuel. After complete dilution of the starting materials and fuel in distilled water, the solution was heated (under magnetic stirring) on a hot plate at around 100 °C until water evaporation and gel formation took place. After that, the mixture was continuously heated at around 450 °C until the ignition of the glycine started. Once ignited, the gel underwent a combustion process and yielded voluminous $La_{0.7}Ca_{0.3}Mn_{1-x}Ni_xO_3$ powders. The obtained powders were then calcined in air at 700 °C for 3 h in order to remove the unreacted carbon compounds and the organic material. The combustion reaction can be expressed as:

$$0.7La(NO_3)_3 + 0.3Ca(NO_3)_2 + (1-x)Mn(C_2H_3O_2)_2 + xNi(NO_3)_2 + yC_2H_5NO_2 \rightarrow La_{0.7}Ca_{0.3}Mn_{1-x}Ni_xO_3 + aCO_2 + bN_2 + cH_2O$$

3. Results and discussion

Before discussing the results achieved in the present investigation, it is of value to mention that the Ni dopants in the perovskite manganite structure were in the +2 valance states [38]. This was verified by sophisticated experimental techniques such as X-ray photoelectron spectra, X-ray absorption fine structure, X-ray absorption near-edge structure, and Fourier transform spectroscopy [31]. Fig. 1(a) shows the XRD patterns of $La_{0.7}Ca_{0.3}Mn_{1-x}Ni_xO_3$ (x = 0, 0.02, 0.07, 0.1) samples recorded at room temperature. It is apparent that the XRD features of the Ni^{2+}-doped samples are the same as those of the pristine compound. It was found that all the samples were single-phase with an orthorhombic perovskite crystalline structure. No evidence of structural phase transformation was found when the Ni^{2+} doping level in LCMO was changed. These findings suggest that the auto-combustion method is an efficient, time-saving and inexpensive route for preparing high-quality LCMO powders with Ni^{2+} doping levels up to 10%. An enlarged scale of the most intense peak (200 Bragg reflection) of the XRD patterns shows a shift to lower 2θ values (Fig. 1(b)), indicating that the cell parameters (and thus the unit cell volume) increasewith increasing Ni^{2+} content. Note also that the full width at half maximum (FWHM) for the most intense peak increases with an increase in the Ni^{2+} content, and consequently the average grain size should decrease. The full profile fits, using the GSAS program, to the XRD spectra for the $La_{0.7}Ca_{0.3}Mn_{1-x}Ni_xO_3$ samples are shown in Fig. 1(a). A perfect convergence of the experimental and the calculated data was obtained. As a result, the crystal structure was indexed in the orthorhombic system

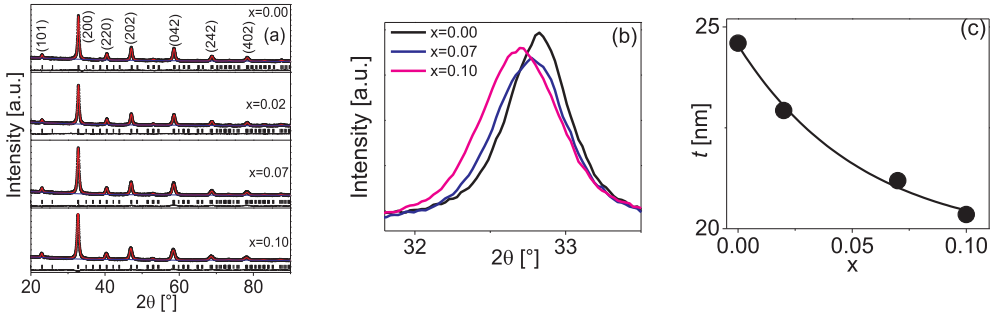

Fig. 1. (a) X-ray diffraction patterns for $La_{0.7}Ca_{0.3}Mn_{1-x}Ni_xO_3$ (x = 0, 0.02, 0.07, 0.1) samples. Refined profiles and difference profile are shown at the bottom. (b) (200) Bragg reflection plotted on enlarged scale. (c) Average particle sizes of the samples obtained from the Rietveld refinement.

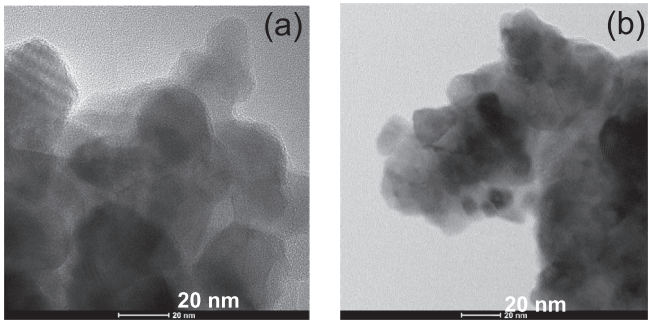

Fig. 2. TEM image of the pristine LCMO sample.

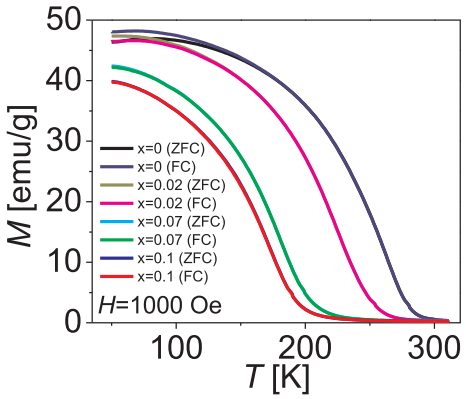

Fig. 3. Temperature dependence of the field-cooled (FC) and zero-field-cooled ZFC magnetization for $La_{0.7}Ca_{0.3}Mn_{1-x}Ni_xO_3$ (x = 0, 0.02, 0.07, 0.1) samples recorded at H = 1000 Oe.

with the Pbnm space group. The results of the Rietveld refinement have been reported elsewhere [39]. In short, all the cell parameters and the volume exhibit a tendency to grow as the Ni^{2+} content increases. This result is consistent with the fact that the ionic size of Ni^{2+} (0.69 Å) is slightly larger than those of Mn^{3+} (0.645 Å) and Mn^{4+} (0.53 Å) [40]. The observed variation of the LCMO cell parameters upon Ni doping also suggests that the Ni ions are mainly in the Ni^{2+} state and that they replace Mn^{3+} ions. The average particle sizes of the samples, calculated from the Rietveld refinement, were 24.6, 22.9, 21.2, and 20.3 nm for x = 0, 0.02, 0.07, and 0.1, respectively (Fig. 1(c)). A systematic decrease in the grain size upon Ni^{2+} doping is clearly evidenced, which is in accordance with the increase in the FWHM values observed in Fig. 1(b). Fig. 2 shows the microstructure of the parent LCMO sample obtained from the TEM analysis. The images show that that the morphology of the compound consists of homogenous particles (rounded polyhedrons) with the grain boundaries clearly visible. The particles are abundant and almost uniform in size. The average particle size of the sample observed from the TEM micrograph varies between 20 and 30 nm and is in reasonable agreement with the crystallite size obtained from the XRD patterns. The variation in the grain size, as well as the grain boundaries, will result in a variation of the bond angle, which affects the DE interaction. Consequently, the orbital overlap and hopping of electrons is reduced [41].

In order to determine the influence of the structural and electronic changes generated by the Ni^{2+} doping on the magnetic and magnetocaloric properties of the $La_{0.7}Ca_{0.3}Mn_{1-x}Ni_xO_3$ samples, magnetization measurements versus T and H were performed. Fig. 3 shows the temperature dependence of the field-cooled (FC) and zero-field-cooled ZFC magnetization $M(T)$ of the synthesized $La_{0.7}Ca_{0.3}Mn_{1-x}Ni_xO_3$ (x = 0, 0.02, 0.07, 0.10) nanopowders under an applied field of 0.1 T. All the samples showed a smooth magnetic transition from the paramagnetic (PM) to the ferromagnetic (FM) state as T decreased. The value of T_C was systematically reduced from 260 to 180 K for x = 0 and x = 0.1, respectively. On the basis of the double-exchange (DE) mechanism, an increase in the Ni^{2+} content leads to the formation of a larger proportion of Mn^{4+} with respect to Mn^{3+} [42]. The change in the Mn^{3+}/Mn^{4+} ratio weakens the DE, and therefore magnetization and T_C are reduced. In addition, the competition between FM and AFM exchange interactions is reinforced [34]. In particular, the AFM interaction between different Mn-Mn, Mn-Ni, and Ni-Ni pairs increases, due to the increase in Mn^{4+} caused by the appearance of Ni^{2+} ions in the LCMO lattice [31]. More precisely, the substitution of Mn^{3+} with Ni^{2+} ions can reduce the number of available hopping sites and create cuts in the conduction path, which weakens the DE interaction.

In many papers, it has been demonstrated that the reduction in particle size has a direct consequence for the magnetic properties of novel oxides [43–46]. The existence of a surface layer, the so-called magnetically dead layer, due to a non-collinear spin arrangement at the surface of the crystallites, was first postulated in Ref. [47]. The thickness of this surface layer increases when reducing the particle size, and consequently the saturation magnetization M_s decreases [47], as observed in Fig. 3. A core/surface discrimination was then suggested, where the magnetic coupling on the surface is lower than that expected in the core. As a result, the transition is enlarged and the overall T_C reduced [43]. The reduction of the magnetization and the T_C upon an increase in the Ni^{2+} content is in good agreement with the reduction of the average grain size of the Ni^{2+}-doped LCMO samples. Thus it is apparent that the role of a nonmagnetic surface layer becomes more relevant as the average grain size decreases [30]. The reduction of the T_C with the increase in the Ni^{2+} doping level can also be explained by considering the reduction of the effective e_g electron bandwidth W [48]. The decrease in the W value reduces the overlap between the Mn_{3d} and the O_{2p} orbitals, which in turn decreases the exchange interaction between Mn^{3+}-O^{2-}-Mn^{4+} ions. The reduction in the exchange interaction strength reduces the FM coupling between neighboring manganese ions, leading to a reduction in the T_C.

In order to evaluate the MC effect in the Ni^{2+}-doped samples, the magnetic-field dependence of the magnetization, $M(H)$, was measured for the different samples. Fig. 4(a) and (c) show the $M(H)$ curves for

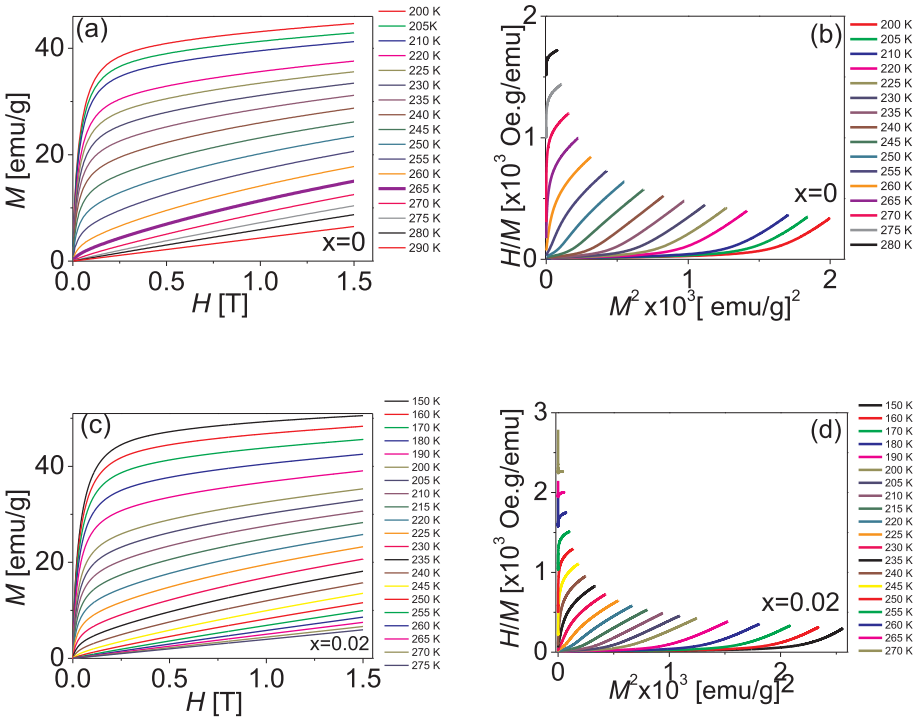

Fig. 4. Isothermal magnetization curves for $La_{0.7}Ca_{0.3}Mn_{1-x}Ni_xO_3$ samples with x = 0 (a) and x = 0.02 (c) samples measured in magnetic field strengths varying between 0 and 1.5 T. The temperature increment is 5 K for the range around T_C. Arrott plots (H/M versus M^2) of the samples $La_{0.7}Ca_{0.3}Mn_{1-x}Ni_xO_3$ with x = 0 (b) and x = 0.02 (d) around their FM-PM phase transition T_C.

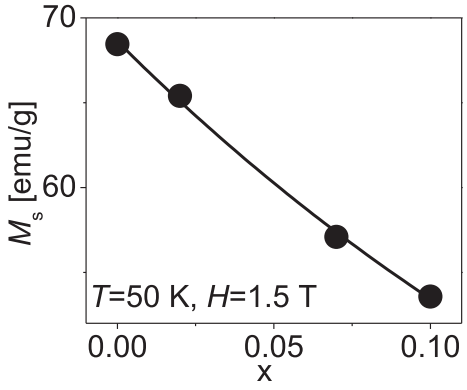

Fig. 5. Variation of the highest magnetization with the Ni^{2+} concentration for $La_{0.7}Ca_{0.3}Mn_{1-x}Ni_xO_3$ (x = 0, 0.02, 0.07, 0.1) samples at T = 50 K and H = 1.5 T.

representative x = 0 and x = 0.02 samples recorded at different temperatures near T_C in the field range of H = 0–1.5 T. The $M(H)$ curves indicate that the magnetization of the samples increases rapidly at low fields and then tends to saturate at higher fields, which reflects the magnetic behavior of LCMO. The curves do not reach saturation values at fields as strong as 1.5 T, which can be attributed to the competition between the FM and AFM interactions. For both samples, at a specific field H, M decreases gradually with increasing temperature, in good agreement with the trend of the $M(T)$ data. This decrease is primarily due to the thermal agitation, which disrupts the arrangement of the magnetic moments. The nonlinear $M(H)$ curves in the FM region become linear in the PM region. Moreover, it can be seen in Fig. 5 that the magnitude of the magnetization at 50 K and 1.5 T decreases monotonically with increasing Ni^{2+} content.

The nature of the magnetic phase transition in the $La_{0.7}Ca_{0.3}Mn_{1-x}Ni_xO_3$ (x = 0, 0.02) samples is determined by plotting the Arrott plots H/M versus M^2 curves (Fig. 4(b) and (d), respectively). Near the T_C, all the curves exhibit a positive slope, indicating that the PM-FM phase transition is second-order according to Banerjee criteria [49]. Although most mixed-valence manganites such as $La_{0.7}Ca_{0.3}MnO_3$ are associated with the first-order character of the magnetic transition [50], changes of the magnetic phase transition order can be induced when the particle size is brought down from bulk to a few tens of nanometers range [51]. In this case, there will be a large number of spins on the surface of nanoparticles that are generally expected to be disordered and will lead to destruction of any spin order [52]. This so-called core/shell morphology model predicts that the disordered outer layer is more likely to undergo a second-order transition, from the disordered state to the paramagnetic one [53]. In this way, it is very probable that the observed second-order magnetic phase transition in the parent LCMO sample is linked to the effects of the downsizing of the particle.

In order to evaluate how the Ni^{2+} doping influences the MC effect in LCMO, the magnetic entropy change (ΔS_M) in the second-order magnetic phase transition, arising when the applied magnetic field changes from 0 to H, and the relative cooling power (RCP) must be calculated. Based on thermodynamic theory, ΔS_M can be derived from the thermodynamic Maxwell relation $\left(\frac{\partial S}{\partial H}\right)_T = \left(\frac{\partial M}{\partial T}\right)_H$. By taking the $M(H,T)$ data, ΔS_M of the samples can be evaluated through the relation $-\Delta S_M(T, \Delta H) = S_M(T, H) - S_M(T, 0) = -\int_0^H \left(\frac{\partial M}{\partial T}\right)_H dH$ [54]. In the present case, the magnetization is measured at small discrete fields (ΔH = 40 Oe) and temperature intervals (ΔT = 5 K). Under these conditions, the integral in the preceding equation can be numerically approximated as follows: $\Delta S_M(T, \Delta H) = \sum \frac{M_i - M_{i+1}}{T_i - T_{i+1}} \Delta H_i$ [34], M_i and M_{i+1} being the magnetization values measured at T_{i+1} and T_i temperatures at a magnetic field change ΔH [55]. In turn, the RCP values are determined by means of the relation $RCP = -\int_{T1}^{T2} \Delta S_M(T) dT$, where T_1 and T_2 are defined as the temperature at the cold and hot ends, respectively, of an ideal thermodynamic cycle. For practical purposes, the RCP value can be evaluated using the equivalent relation $RCP = |\Delta S_{M,max}| x \delta T_{FWHM}$ [55]. Here, δT_{FWHM} represents the full width at half maximum of the magnetic entropy change curve. Fig. 6 shows typical temperature dependences of $-\Delta S_M$ for representative samples with x = 0 and x = 0.02 at magnetic field strengths varying between 0.25 and 1.5 T. Results for the other Ni^{2+} concentrations ($-\Delta S_{M,max.}$ values) are plotted in Fig. 7(a). It can be seen in Fig. 6 that $-\Delta S_M$

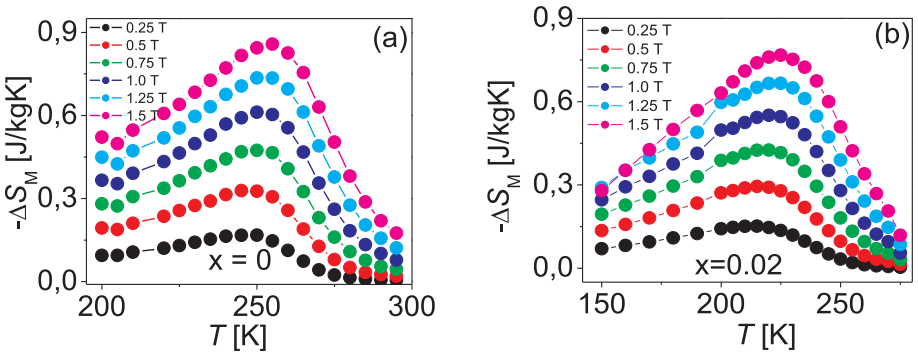

Fig. 6. Magnetic entropy change ΔS_M as functions of temperature and magnetic field for the undoped and 2% Ni^{2+}-doped LCMO samples.

reaches its maximum value at around the respective T_C of each sample. Moreover, $-\Delta S_M(T)$ increases when increasing H, and the $-\Delta S_{M,max.}$ position shifts slightly towards higher temperatures. A similar trend was observed for the x = 0.07 and x = 0.1 samples (not shown). The RCP values obtained for the LCMO samples with different Ni^{2+} doping levels in the different magnetic fields are shown in Fig. 7(b). It can be seen in Fig. 7(a) that the value of $|\Delta S_{M,max}|$decreases upon Ni^{2+} doping. A marked reduction of the maximum entropy upon Ni^{2+} doping has also been reported for the $La_{0.7}Sr_{0.3}Mn_{1-x}Ni_xO_3$ (x = 0.1, 0.33) system [56]. A similar behavior has been reported for $La_{0.7}Sr_{0.3}Mn_{1-x}M_xO_3$ (M = Cr, Fe, and Co) manganites [57–59]. Although the addition of Ni^{2+} reduces the $|\Delta S_{M,max}|$, the RCP value is increased as compared to that of the parent LCMO (Fig. 7(b)). Thus the reduced $|\Delta S_{M,max}|$ values are compensated for by increased δT_{FWHM} values for each magnetic field, resulting in an enhanced RCP over sharper transitions [60]. It is interesting to consider the case of thin films, for which a strong drop in the $|\Delta S_{M,max}|$ value has been reported [61]. Nevertheless, the strong drop in the $|\Delta S_{M,max}|$ value was compensated for by the increased breadth of the transition. Thus large RCP values are often encountered in materials in thin film form. From the results obtained in the present study and by considering those reported in a variety of publications [56], it is possible to assert that the MCE in perovskite manganites is certainly large. In particular, it is demonstrated in the present study that the RCP of the sample with x = 0.02 is increased by about 90% of that of the parent LCMO. This is certainly a promising result for practical applications of manganites in magnetic refrigeration technology over a wide range of operating temperatures.

The ΔS_M can be calculated from the specific heat capacity by using the thermodynamic relation $\Delta S_M = \int_0^T \frac{C_p(T,H)-C_p(T,0)}{T} dT$ [55]. Hence the relation $\Delta C_p = C_p(T, H) - C_p(T, 0) = T\left(\frac{\partial \Delta S_M}{\partial T}\right)$ allows one to estimate the change of the specific heat ΔC_p induced by the magnetic field variation. Fig. 8 shows the variation of the C_p with the temperature for $La_{0.7}Ca_{0.3}Mn_{1-x}Ni_xO_3$ (x = 0, 0.02, 0.07, 0.1) samples recorded at 0.5 T. It can be seen in Fig. 8 that the ΔC_p values change from the negative to the positive in the vicinity of T_C for each Ni^{2+} doping level.

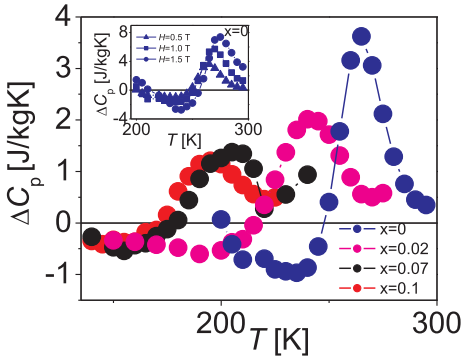

Fig. 8. Variation of C_p of the $La_{0.7}Ca_{0.3}Mn_{1-x}Ni_xO_3$ (x = 0, 0.02, 0.07, 0.1) samples as a function of temperature at H = 0.5 T. Inset: Temperature dependence of C_P of the pristine LCMO sample recorded at H = 0.5, 1.0 and 1.5 T.

Moreover, the minimum value of ΔC_p increases with the applied field and the position shifts to higher temperatures (inset of Fig. 8). The behavior of ΔC_p is related to the relatively broad PM-FM transition exhibited by the nanometric $La_{0.67}Ca_{0.33}Mn_{1-x}Ni_xO_3$ samples [Fig. 3]. The sum of the two parts is the magnetic contribution to the total specific heat, which affects the cooling or heating power of the magnetic refrigerator [62]. The appearance of negative values for C_p should be interpreted carefully, because negative values of C_p do not make physical sense. The issue of having negative values for C_p can be tackled by considering that the use of magnetocaloric materials in magnetic solid-state refrigeration requires a high C_p in order to reduce oscillations in temperature during the alternations in the transfer of heat flow. Nevertheless, this value should not be too high, since this will tend to reduce the adiabatic temperature change (ΔT_{ad}) of a magnetic system when the magnetic field is varied from 0 to H_{max}. Mathematically, ΔC_p should differ from zero only in the vicinity of T_C. In this regard, the C_p values are positive before the transition ($T > T_C$) and negative after the transition ($T < T_C$). Since the first derivative $\partial M/\partial T < 0$ around T_C, the basic equation relating S_M and M gives values of $S_M < 0$, and

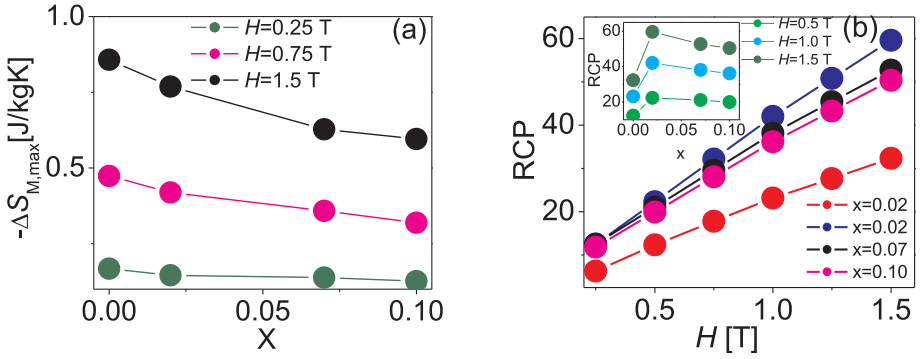

Fig. 7. (a) Variation of the $\Delta S_{M,max.}$ values with the Ni^{2+} concentration at different magnetic fields for $La_{0.7}Ca_{0.3}Mn_{1-x}Ni_xO_3$ (x = 0, 0.02, 0.07, 0.1) samples. (b) Dependence of the RCP values on the magnetic field for $La_{0.7}Ca_{0.3}Mn_{1-x}Ni_xO_3$ (x = 0, 0.02, 0.07, 0.1) samples. Inset: RCP values versus Ni^{2+} content at three different magnetic fields.

accordingly the total entropy decreases upon magnetization. Hence a sharp variation in ΔC_p values is expected at $T = T_C$.

As seen in Fig. 3, the LCMO samples synthesized by the auto-combustion method exhibit a second-order PM-FM phase transition. In order to understand the field dependence of ΔS_M, the magnetocaloric response of a system should be modeled. This can be can be approached by developing first-principles models for particular materials. A variety of predictions can be carried out for a particular alloy by means of these models (e.g. mean-field models). Nevertheless, discrepancies between the predictions of the models and the experimental $\Delta S_M(H)$ data in materials with a second-order magnetic phase transition have demonstrated that additional models are necessary to explain the $\Delta S_M(H)$ dependence. Fortunately, the existence of an universal curve for the $\Delta S_M(H)$ dependence in materials with a second-order phase transition has recently been demonstrated [63]. Such a curve can be constructed phenomenologically without knowing the critical exponents of the material or its equation of state [63]. This universal curve is not restricted to the mean-field case. Here, the different $\Delta S_M(T,\Delta H)$ curves recorded at several magnetic fields should collapse into a single master curve with the scaling of the temperature. In order to plot such a universal curve, the different $\Delta S_M(T,\Delta H)$ curves should be normalized with respect to their respective $\Delta S_{M,max.}$ values. In addition, the temperature axis should be rescaled in a different way below and above T_C, as follows: $\theta = \begin{cases} \frac{-(T-T_C)}{T_{r1}-T_C}, & T \le T_C \\ \frac{(T-T_C)}{T_{r2}-T_C}, & T \ge T_C \end{cases}$ [63]. Here, T_{r1} and T_{r2} are reference temperatures corresponding to a certain fraction $f = \Delta S_M(T_{r1,2})/\Delta S_{M,max}$. The choice of f (with $0 < f < 1$) does not affect the universal curve construction. Normalized entropy-change curves as a function of the rescaled temperature theta at different applied fields for representative $La_{0.7}Ca_{0.3}Mn_{1-x}Ni_xO_3$ (x = 0, 0.02) samples are shown in Fig. 9. A superposition of the data into a single curve both in the PM region with $\theta > 0$ and the FM region with $\theta < 0$ can clearly be seen for all the studied samples. Similar behavior was verified for samples with higher Ni^{2+} doping levels (not shown). The collapse of $\Delta S_M(T,\Delta H)$ into a unique curve, within a wide temperature range, is a confirmation of the general validity of the treatment in the second-order phase transition compounds. Thus the order of the phase transition of materials can be determined by means of the universal curve. This is especially useful when the purely magnetic Banerjee criterion gives erroneous results. Furthermore, the universal curve can be used for practical purposes, such as making extrapolations of the results up to fields or temperatures not available in the laboratory, enhancing the resolution of the data, and deconvoluting the response of overlapping magnetic transitions [64].

Since the second-order transition has been proved for all the $La_{0.7}Ca_{0.3}Mn_{1-x}Ni_xO_3$ samples, it is to be expected that the magnetic field dependence of ΔS_M will vary according to the relation $\Delta S_M = a(H)^n$, where a is a constant and n a magnetic-state-dependent exponent [65]. The exponent n, which depends on temperature and field, can be locally calculated as $n = \frac{dln|\Delta S_M|}{dlnH}$. The variation of ΔS_M as a function of

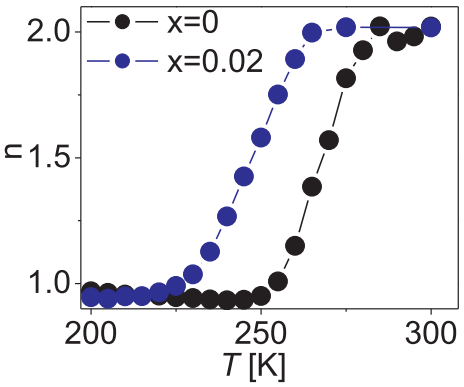

Fig. 10. Temperature dependence of the field exponent n for LCMO samples with x = 0 and x = 0.02 obtained at $H = 1$ T.

H around the T_C is well described by a power relation, and n values of 0.87, 0.88, 0.82, and 0.82 were obtained for $La_{0.7}Ca_{0.3}Mn_{1-x}Ni_xO_3$ samples with x = 0, 0.02, 0.07, and 0.1, respectively [37]. The temperature dependence of n is displayed in Fig. 10 for representative LCMO samples with x = 0 and x = 0.02. The evolution of the $n(T)$ curves resembles that predicted by the mean field model [66]. At temperatures below T_C (FM state of the material), n has values approaching 1. This indicates that although the magnetization curves depend on the temperature at these temperatures, the $n(T)$ dependence is essentially field independent. At temperatures above T_C (PM state of the material), n approaches 2 as a consequence of the Curie–Weiss law [67]. At $T = T_C$, values of $n \approx 0.9$ are found for the two representative compositions. Within the framework of mean-field theory, a value $n = 0.67$ is predicted at T_C [68]. The deviation of n from the mean-field theory value suggests the existence of magnetic inhomogeneities and/or superparamagnetic clusters in the vicinity of T_C in the compounds. Mean-field theory applied to SOMT inhomogeneous ferromagnets has produced n values different from 0.67 [67,69]. It is evident that further work should be done in order to obtain deeper insight into the nature of the magnetic interactions in the $La_{0.7}Ca_{0.3}Mn_{1-x}Ni_xO_3$ system. Concretely, it is necessary to study the associated critical exponents in detail for this SOFM material.

Perovskite LCMO manganites are important not only because of their elastic [70], structural, electronic, and magnetic transition [71] properties but also because of their extraordinary colossal magnetoresistance (CMR) property. Interestingly, the MR and the MC effects in manganites are usually observed around the FM-PM phase transition [72]. Hence the existence of a close relationship between the electrical and magnetic properties in LCMO, namely a change in resistivity and magnetic entropy, is anticipated. Certainly in the framework of the double-exchange theory the electrons tend to hop between Mn ions of different valences while keeping their spins unchanged. Therefore, when the arrangement of the spins of the Mn ions is modified by an

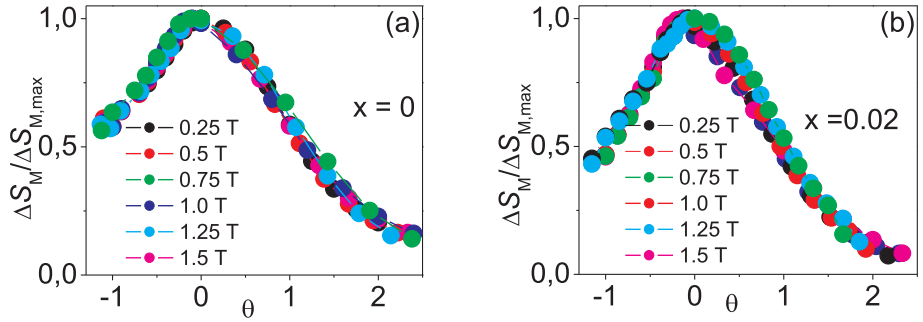

Fig. 9. Normalized magnetic entropy change as a function of the rescaled temperature θ for the samples $La_{0.7}Ca_{0.3}Mn_{1-x}Ni_xO_3$ samples with x = 0 (a) and x = 0.02 (b).

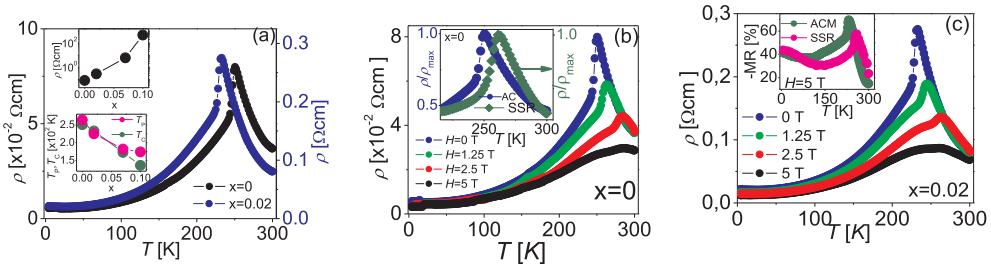

Fig. 11. (a) Dependence of the resistivity on the temperature for $La_{0.7}Ca_{0.3}Mn_{1-x}Ni_xO_3$ (x = 0, 0.02) samples measured at $H = 0$ T. Top inset: variation of the resistivity maximum of the $La_{0.7}Ca_{0.3}Mn_{1-x}Ni_xO_3$ samples with the Ni^{2+} content. Low inset: Plot of T_C and T_P versus Ni^{2+} content for $La_{0.7}Ca_{0.3}Mn_{1-x}Ni_xO_3$ (x = 0, 0.02, 0.07, 0.1) samples. (b) Temperature variation of the resistivity at $H = 0$, 1.25, 2.5, and 5 T of the pristine LCMO sample. Inset: ρ(T) dependences at $H = 0$ T for pristine LCMO samples synthesized by auto-combustion (AC) and standard solid-state reaction (SSR). (c) Temperature variation of the resistivity at $H = 0$, 1.25, 2.5, and 5 T of the 2% Ni^{2+}-doped LCMO sample. Inset: Variation of the MR with the temperature under a field $H = 5$ T for pristine LCMO samples synthesized by AC and SSR.

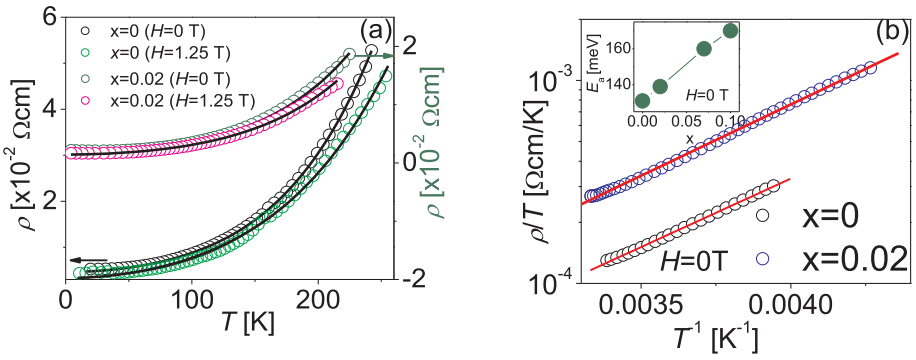

Fig. 12. (a) Representative ρ(T) data measured on $La_{0.7}Ca_{0.3}Mn_{1-x}Ni_xO_3$ samples with x = 0 and x = 0.02 below T_P at $H = 0$ and 1.25 T. The solid lines represent fits of the equation $\rho(T) = \rho_0 + \rho_2 T^2 + \rho_{4.5} T^{4.5}$ to the experimental data. (b) Temperature dependence of the resistivity of the $La_{0.7}Ca_{0.3}Mn_{1-x}Ni_xO_3$ samples with x = 0 and x = 0.02 above T_P at zero magnetic field fitted with the polaron transport model. Inset: activation energy of the polaron as a function of the Ni^{2+}-content.

external field, the resistivity should change simultaneously [72]. In this scenario, the CMR effect in the manganites has been qualitatively understood [73,74]. The interplay between the magnetic and the resistive behavior in manganites, as well as the effect of Ni^{2+} doping on their magnetotransport properties, have been explored in nano-sized $La_{0.7}Ca_{0.}3Mn_{1-x}Ni_xO_3$ samples synthesized via the auto-combustion method. Fig. 11(a) shows the dependence of the resistivity on the temperature, ρ(T), at $H = 0$ for $La_{0.7}Ca_{0.3}Mn_{1-x}Ni_xO_3$ (x = 0, 0.02) samples. It can readily be verified that the resistivity first increases with decreasing temperature and then exhibits a peak around the metal-semiconductor transition temperature T_P (250 and 140 K for x = 0 and x = 0.02, respectively). In addition, the resistivity increases and T_p decreases upon Ni^{2+} doping, as observed in the insets of Fig. 11(a). These effects can be explained on the basis of the DE mechanism (Mn^{3+}–O–Mn^{4+}) [75]. In a manner similar to the magnetic case, the partial substitution of Mn ions with Ni^{2+} leads to a change in the Mn^{3+}/Mn^{4+} ratio [76]. This change, in turn, produces a decrease in DE, evidenced by the decrease in T_p. In short, Ni^{2+} doping suppresses DE because the Mn^{3+}–O–Ni^{2+} bond does not participate in this mechanism [77]. Formation of AFM Ni^{2+}–O–$Ni^{2+}$and Mn^{4+}–O–Mn^{4+} bonds is also possible, which weakens the DE interaction [77,78]. By increasing the Ni^{2+} doping level, the number of AFM bonds may increase, and this would allow one to explain the resistivity increase and the T_p decrease. The increase in the resistivity value of LCMO with the Ni^{2+} content can be also explained in terms of the change in the Mn–O–Mn angle (θ). Indeed, it is known that θ plays a relevant role in the e_g electron mobility [79]. A deviation of θ from 180° increases the distortion, which decreases the transfer integral $t = t_0\cos(\theta/2)$ (here t_0 represents the maximum value of t) [49]. The decrease in the t value decreases the DE interaction between Mn ions [80], and consequently the resistivity increases. Thus an orthorhombic structure with increasing bond distortion results in localized carriers and therefore in higher resistivities. Here, it is worthwhile to note that the T_p values of the samples synthesized via the auto-combustion method are lower than those of the samples obtained via the conventional solid-state reaction. This is clearly evidenced in the inset of Fig. 11(b) for the undoped LCMO samples. The reduction of T_p can be attributed to the downsizing of the particles [23], which can decrease the bond angle and increase its length [81]. This leads to a decrease in the transfer integral, which in turn decreases T_p. By taking the fact that the particle size of the studied samples diminishes with an increase in the Ni^{2+} content (Fig. 1(c)) into account, it is possible to conclude that the substantial increase in the resistivity value is a consequence of the downsizing of the particle. Similar results were reported by Mahesh et al. [23]. The dependence of the resistivity on the temperature measured at different magnetic fields for two representative samples (x = 0, 0.02) is presented in Fig. 11(b) and (c), respectively. The value of the resistivity decreases when a magnetic field is applied, suggesting an existence of the MR effect. The resistivity peak at T_p shifts to higher temperatures with an increase in the magnetic field.

The nature of the conduction in the metallic regime ($T < T_P$) of the $La_{0.7}Ca_{0.3}Mn_{1-x}Ni_xO_3$ samples, both in $H = 0$ T and $H \neq 0$ T, can be examined by means of the equation $\rho(T) = \rho_0 + \rho_2 T^2 + \rho_{4.5} T^{4.5}$ [82]. In this equation, ρ_0 corresponds to the temperature-independent residual resistivity due to domain and grain boundaries, $\rho^2 T^2$ describes the resistivity associated with electron-electron scattering, and $\rho^{4.5} T^{4.5}$ is a term associated with electron-magnon scattering processes due to spin waves. Fig. 12(a) shows the experimental ρ(T) data and the fitting curves for the pristine and the 2% Ni^{2+}-doped LCMO samples below T_P at $H = 0$ and 1.25 T. The good correspondence between the experimental data and the fitting function suggests that the transport mechanism in the metallic regime of the concerned samples is governed by electron-electron and electron-magnon scattering [83]. From the fitting curves, the values of ρ_0, ρ_2, and $\rho_{4.5}$ for the two representative samples are obtained, and the results are listed in Table 1. In the high temperature region ($T > T_p$), the conduction process of the studied samples is well described by the small polaron hopping transport mechanism [84]. In this model, the dependence of the resistivity on the temperature is mathematically represented by the relation $\rho(T) = \rho_0 T\exp(E_a/k_B T)$, ρ_0 being a temperature-independent coefficient, k_B the Boltzmann constant, and E_a the activation energy of the polarons [85]. This function was fit to the experimental resistivity data above T_p for the pristine and the 2% Ni^{2+}-doped LCMO samples. The resulting fitting curves are indicated by the solid lines in Fig. 12(b). A good

Table 1
Fitting parameters for the pristine and the 2% Ni^{2+}-doped LCMO samples. The function $\rho(T) = \rho_0 + \rho_2 T^2 + \rho_{4.5} T^{4.5}$ was fitted to the experimental $\rho(T)$ data recorded in zero field and $H = 1.25$ T.

	$\rho(T) = \rho_0 + \rho_2 T^2 + \rho_{4.5} T^{4.5}$			
x		ρ_0 (Ωcm)	ρ_2 ($\times 10^{-7}$ ΩcmK^{-2})	$\rho_{4.5}$ ($\times 10^{-13}$ ΩcmK$^{-4.5}$)
0	$H = 0$	0.0046	3.65	4.95
	$H = 1.25$ T	0.0033	4.1	2.84
0.02	$H = 0$	0.018	15.7	23.6
	$H = 1.25$ T	0.014	14.7	18.6

concordance between the experimental data and the fitting function can clearly be seen in this plot. Based on the best-fit parameters, the E_a values were determined. The results, plotted in the inset of Fig. 12(b), show that the E_a values increase upon an increase in the Ni^{2+} content. Carrier localization resulting from the electron-phonon interaction has been proposed as possible mechanism behind the increase of E_a [86]. Consequently, higher energies will be required to create free carriers. In this context, results of measurements of $La_{0.7}Sr_{0.3}Mn_{1-x}Ni_xO_3$ (x = 0, 0.025, 0.050, 0.075) ceramics have shown that the small-polaron coupling interaction (γ_{ph}), which is a measurement of electron-phonon interaction, increases with the Ni^{2+} content [86]. Moreover, it has been established that strong electron-phonon interaction can occur for $\gamma_{ph} > 4$ [87]. This requirement was verified for the $La_{0.7}Sr_{0.3}Mn_{1-x}Ni_xO_3$ samples reported in Ref. [86]. The increase of E_a upon an increase in the Ni^{2+} content can also be explained by considering the downsizing of the particles with an increase in the Ni^{2+} content, as verified by XRD analysis (Fig. 1(c)). Although the downsizing of the particles may increase the interconnectivity between grains during the sintering process, the number of grain boundaries increases considerably in nano-sized systems. This, in turn, will hamper the possibility of the conduction electron hopping to neighboring sites [88]. Thus the conduction bandwidth will decrease, and as a result, the value of E_a will increase. The results reported in the present paper suggest that the conduction bandwidth of the materials may be modified by tuning their particle size. Similar conclusions have been drawn from studies on other manganites prepared by means of chemical methods, such as the citrate gel technique [89].

The decrease in the resistivity values of the $La_{0.7}Ca_{0.3}Mn_{1-x}Ni_xO_3$ samples with the applied magnetic field was previously demonstrated in Fig. 11(b) and (c). In general terms, the main mechanism responsible for the decrease in the resistivity value upon the application of a magnetic field is its influence on the magnetic domains of the material [90]. Certainty the MR effect can be ascribed to the orientation of the spins in the different domains due to the presence of the magnetic field. When the spin system is oriented, the carrier scattering during the hopping processes is eliminated [86]. Fig. 13 shows the dependence of the MR on the temperature, recorded at 1.25 T, for $La_{0.7}Ca_{0.3}Mn_{1-x}Ni_xO_3$ (x = 0, 0.02) samples. Two MR effects can be seen in the MR(T) curves of the studied samples. The first occurs near T_P, with maximum values of MR 45% for $H = 1.25$ T. This MR is due to the DE interaction of Mn^{3+}-Mn^{4+} pairs [90]. The other notable variation occurs at low temperatures below ~100 K. In this region, the values of the MR increase with decreasing temperature, resembling the MR spin-polarized tunneling effect in granular ferromagnetic systems [91]. This behavior can be described by a Curie-Weiss law-like, $a + b/(c + T)$ [92]. The MR(T) data for the undoped and 2% Ni^{2+}-doped LCMO samples at low temperatures are shown in the inset of Fig. 13. The function $a + b/(c + T)$ has been fit to the experimental data, and the corresponding a, b, and c parameters are listed in Table 2. It is also noteworthy that the value of the MR near the peak of the pristine and the 2% Ni^{2+}-doped LCMO samples does not show a significant change at $H = 1.25$ T. Both samples exhibit sharp and equally intense peaks

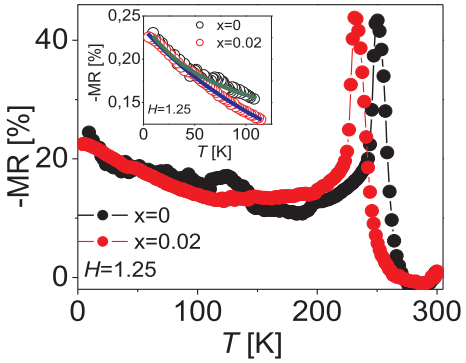

Fig. 13. Variation of the MR with the temperature at $H = 1.25$ T for $La_{0.7}Ca_{0.3}Mn_{1-x}Ni_xO_3$ samples with x = 0 and x = 0.02. Inset: MR(T) data for $T < 120$ K fitted to a Curie-Weiss law-like, $a + b/(c + T)$. The solid lines in the inset correspond to the fitting curves.

Table 2
Fitting parameters for the pristine and 2% Ni-doped LCMO samples obtained from fits of the $a + b/(c + T)$ equation to the experimental MR-data recorded at $H = 1.5$ T.

	x = 0	x = 0.02
a	0.09125	−0.1008
b (K)	12.223	84.882
c (K)	80.785	252.579

around T_C. The insensitivity of the MR to the 2% Ni^{2+} doping is observed even at higher fields (Fig. 14(a)). The results shown in Figs. 13 and 14(a) demonstrate that the MR of LCMO is not much affected by Ni^{2+} doping levels as high as 2%. Nevertheless, a significant increase in the MR value is verified for higher Ni^{2+} doping levels. The increase of the MR value with an increase in the Ni^{2+} content may be explained by considering the concomitant reduction of the particle size of the doped samples. Thus the latter results suggest that manganites having nanometer-sized particles can exhibit larger MR around T_C than ones with a higher particle size. This can be directly verified by comparing the samples prepared via two different routes, namely auto-combustion and standard solid-state reaction. As is widely known, the grain size of LCMO samples synthesized by means of the physical method is in the micrometric range. The inset of Fig. 11(c) shows the dependence of the MR on the temperature for pristine LCMO samples fabricated via the two different routes. It is evident that the MR (at $T \sim T_C$) of the sample synthesized through auto-combustion is higher than that of the sample synthesized via solid-state reaction. Generally speaking, it is expected that a substantial contribution by the grain boundaries be present in these nanometric-sized systems [14]. The dependence of the MR on the external magnetic field at different temperatures for the $La_{0.7}Ca_{0.3}Mn_{1-x}Ni_xO_3$ (x = 0, 0.02) sample is displayed in Fig. 14(b) and (c). It can be seen in this plot that the highest values of MR occur around the T_C of each sample, as already seen in Fig. 13. It can also be verified that the MR decreases after the transition passes T_p and starts to increase at $T < 100$ K. Interestingly, a sharply increasing nature of the magnitude of the MR is observed at low temperatures within a narrow range of magnetic field strengths ($H < \pm 1$ T). At a higher field ($H > 1$ T), the variation of the MR is slower and almost linear with an increasing magnetic field. As previously mentioned, the behavior of the MR at low temperatures resembles that of typical ferromagnetic granular materials at low temperatures. Indeed, the sharp drop of the MR can be explained by taking the intergranular spin-polarized tunneling of electrons near the grain boundaries into account. This kind of MR is known as extrinsic MR, and in general the extrinsic nature of MR is frequently found at low magnetic fields [93]. However, it has been argued that the high-field response is also due to the existence of the

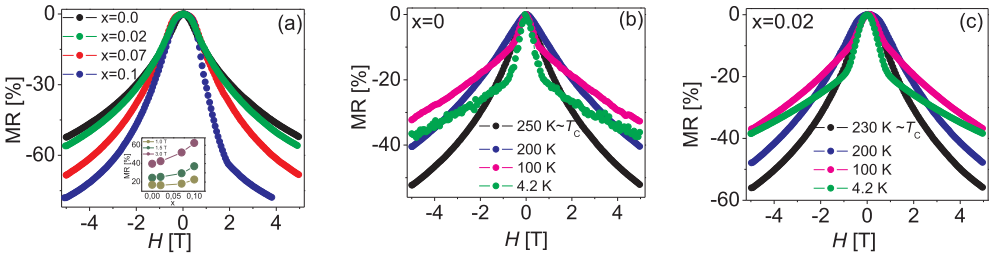

Fig. 14. (a) Variation of maximum MR ($T = T_C$) as a function of the magnetic field for $La_{0.7}Ca_{0.3}Mn_{1-x}Ni_xO_3$ (x = 0, 0.02, 0.07, 0.1) samples Inset: MR versus Ni^{2+}-content recorded at H = 1.0, 1.5 and 2 T. (b) MR(H) curves at different temperatures for the pristine LCMO sample. (c) MR(H) curves at different temperatures for the 2% Ni^{2+}-doped LCMO sample (c).

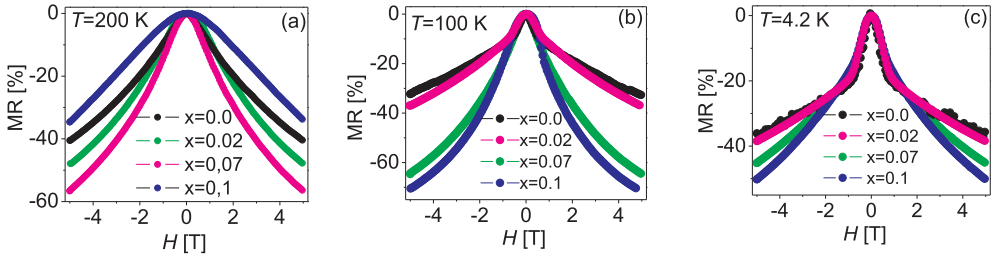

Fig. 15. Variation of the MR with the external magnetic field for the $La_{0.7}Ca_{0.3}Mn_{1-x}Ni_xO_3$ (x = 0, 0.02, 0.07, 0.1) samples at T = 200 K (a), T = 100 K (b) and T = 4.2 K (c).

grain boundary [91]. The nature of the grain boundary is the key ingredient in the mechanism of the electrical transport, as it constitutes the barrier through which carriers tunnel. The application of an external magnetic field brings about the movement of the magnetic domain walls through the grain boundaries. This movement is associated with the progressive alignment of magnetic domains, and as a result, a sharp drop of MR at low fields is commonly observed [91].

Fig. 15 shows the variation of the MR with the external magnetic field for the $La_{0.7}Ca_{0.3}Mn_{1-x}Ni_xO_3$ (x = 0, 0.02, 0.07, 0.1) samples at different temperatures (200, 100, 4.2 K). It can be seen that the value of the MR for the Ni^{2+}-doped samples, at $H \geq 1$ T, is higher than that of the pristine LCMO sample (the lower MR value seen for the sample with x = 0.1 at 200 K is due to its reduced $T_C \sim 170$ K). The improvement of the MR with Ni^{2+} doping at low magnetic fields (H = 1 T) and temperatures around T_C has been already corroborated (inset of Fig. 14(a)). These results indicate that the MR of LCMO can be considerably improved upon Ni^{2+} doping. It is evident that the value of the MR depends on the temperature and the magnetic field strength. The increased value of the MR at low fields (H = 1 T) and $T \approx T_C$, as compared to the pristine LCMO, suggests a higher magnetic field sensitivity of the Ni^{2+}-doped samples due to enhanced tunneling of electrons between two grains through the grain boundary. In the pristine LCMO samples, the electrons are spin polarized in the LCMO grains, and charge transport occurs between Mn ions. In the case of the Ni^{2+}-doped samples, the downsizing of the particles leads to an increased number of grain boundaries. Consequently, the highest spin-dependent scattering takes place at the grain boundaries, resulting in higher resistivity, as previously observed in the inset of Fig. 11(a). When an external magnetic field is applied, the domains are aligned, and therefore the spin disorder near the grain boundary region is reduced. Hence the spin-polarized tunneling is enhanced, which results both in higher MR values and in a higher magnetic field sensitivity of the Ni^{2+}-doped LCMO samples.

It is a known fact that magnetic entropy is also a parameter usually used to characterize magnetic order [94]. By taking into account that the magnetic disorder has a strong effect on the resistive behavior of the manganites, a clear relation between ΔS_M and resistivity is expected [95]. This is certainly verified for the LCMO samples synthesized via the auto-combustion method. The qualitative relation between these two quantities is seen in Fig. 16 for the pristine LCMO sample. As expected, the MR and ΔS_M peaks appear simultaneously. Nevertheless, it is evident that the temperature dependences of these physical quantities are

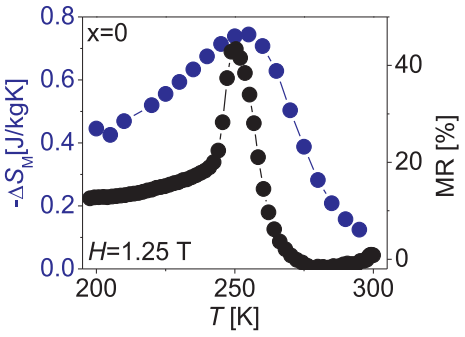

Fig. 16. Comparison of ΔS_M and MR of the pristine LCMO sample under a field of 1.25 T.

different. Indeed, MR shows a sharp drop when the temperature decreases from T_C, whereas the variation of ΔS_M is smooth below T_C. This finding suggests that the relation between ΔS_M and MR is not simple. The ΔS_M and MR peaks around T_C have a common origin, namely the spin order/disorder feature around T_C. As stated above, the MR results from spin disorder suppression. The different shapes of the ΔS_M and MR curves, particularly the difference in broadness, might be understood by considering that spin disorder suppression is not the only mechanism responsible for the MR effect. Concretely, the MR observed around T_C is not completely brought about by spin disorder suppression. Other contributions, arising from sophisticated effects such as Jahn–Teller distortion [96] and electronic phase separation [97], have also been considered as plausible explanations for the colossal magnetoresistance in manganites. The deviation between MR and $\Delta S_M(T)$ behavior at low temperatures is related to the mechanism responsible for the MR in this temperature range. Indeed, spin disorder suppression in this temperature range is inoperative. As discussed previously, at low temperatures, the granular nature of the compound leads to carrier transport through spin-dependent tunneling between grains, which results in a large low-field MR [91]. Here, it is worthwhile to mention that the magnetic spin disorder that characterizes ΔS_M is high around T_C and leads to magnetic polaron formation that affects carrier transport and hence the resistivity ρ [95]. At low temperatures, the ferromagnetic ordering results in magnetic polaron suppression. Thus the ferromagnetic ordering at low temperatures excludes the impact on the MR by magnetic polarons, due to the absence of magnetic spin disorder that characterizes ΔS_M. This also explains the deviation between ΔS_M and MR behavior at low

temperatures. The absence of a simple relation between MR and ΔS_M spurred the search for more suitable models to explain the discrepancy. In a very interesting investigation, Xiong et al. [95] considered that the relation between these two quantities, if it exists, should be in the form of a logarithm. Such a function can smoothen the steep jump of MR near T_C and amplify the variation of MR far below this temperature. However, it was found that a simple logarithmic relation could not describe the dependence of ΔS on MR. Finally, the relation between ΔS_M and ρ was found, and it reads $\Delta S = -\alpha \int_0^H \left[\frac{\partial \ln(\rho)}{\partial T}\right] dH$. The latter relation has been successfully applied to describe the relation between the two quantities in a variety of manganites. In the case of the nanometric $La_{0.7}Ca_{0.3}Mn_{1-x}Ni_xO_3$ samples reported in the present paper, the relation between ΔS_M and ρ will be carefully explored using the cited relation, and the results will be reported in a forthcoming paper.

4. Conclusions

$La_{0.7}Ca_{0.3}Mn_{1-x}Ni_xO_3$ (x = 0, 0.02, 0.07, 0.10) ceramic powders with particle size in the nanometric range were successfully obtained by means of the auto-combustion reaction, and their magnetocaloric and magnetotransport properties were carefully analyzed. The introduction of Ni^{2+} ions into the Mn site of pristine LCMO samples decidedly influenced their structural, magnetocaloric, and magnetotransport properties. The reduction of the T_C of the nanometric LCMO as compared to the bulk counterpart is attributed to the presence of a surface layer, which destabilizes the magnetic order. The performance of the magnetocaloric effect of the LCMO samples is significantly increased upon Ni^{2+} doping. In this regard, the LCMO sample with a Ni^{2+} doping level as low as 2% featured a ~90% increase in the RCP value at 1.5 T applied magnetic field. This feature is indeed desirable for practical applications in magnetic refrigeration. The observed increase in the value of the resistivity with the Ni^{2+} doping can be attributed to the DE decrease, which hampers the movement of the e_g band electron of Mn. The resistivity in the ferromagnetic metallic region seemed to be determined by grain boundary effects, electron-electron scattering, and electron-magnon scattering processes. In the high temperature region ($T > T_C$), the conduction process was explained by the small polaron hopping transport mechanism. Here, the polaron activation energy increased with an increase in the Ni^{2+} content, which could be related to the downsizing of the particles upon Ni^{2+} doping. In general, the application of an external magnetic field drove the metal-insulator transition to higher temperatures and largely depressed the resistivity values. The MR values exhibited maximum values around T_p. MR measurement showed an enhanced field sensitivity for the Ni^{2+}-doped samples as compared to the pristine LCMO ones. In general, the electrical and MR properties of the $La_{0.7}Ca_{0.3}Mn_{1-x}Ni_xO_3$ samples can be explained by the increase in the scattering of the conduction electrons near the grain boundaries. The results suggest that $La_{0.7}Ca_{0.3}Mn_{1-x}Ni_xO_3$ may be regarded as a potential candidate for application in low-field MR devices due to its enhanced magnetic field sensitivity. The MR and ΔS_M peaks appeared simultaneously, suggesting a close relationship between the change in resistivity and magnetic entropy. Nevertheless, the detailed temperature dependence of MR and ΔS_M seemed to be different. Additional factors in the MR mechanism, other than spin disorder suppression, should be taken into account to explain the difference in the behavior of these quantities. The correlation between magnetocaloric and magnetotrasport properties in manganites is an interesting and ongoing theme in condensed matter and deserves additional work and closer analysis.

Acknowledgments

This investigation was supported by Universidad Nacional de Colombia, Medellín Campus. It was also supported by the Spanish Ministry of Economy (Spain) and Competitivity through grants MAT2014-52405-C2-2-R. JPG would also like to acknowledge this ministry for granting a Juan de la Cierva postdoctoral fellowship. A.G acknowledges the financial support of the Departamento Administrativo de Ciencia, Tecnología e Innovación (Colciencias). The authors also want to thank Dr. Francisco Varela Feria at the Centro de Investigación, Tecnología e Innovación (CITIUS) at the Universidad de Sevilla (Spain) for the TEM images.

References

[1] R. Von Helmolt, J. Wecker, B. Holzapfel, L. Schultz, K. Samwer, Giant negative magnetoresistance in perovskite like $La_{2/3}Ba_{1/3}MnO_x$ ferromagnetic films, Phys. Rev. Lett. 71 (1993) 2331.
[2] G. Tang, Y. Yu, W. Chen, Y. Cao, The electrical resistivity and thermal infrared properties of $La_{1-x}Sr_xMnO_3$ compounds, J. Alloy. Compd. 461 (2008) 486.
[3] D.N.H. Nam, N.V. Dai, L.V. Hong, N.X. Phuc, S.C. Yu, M. Tachibana, E. Takayama-Muromachi, Room temperature magnetocaloric effect in $La_{0.7}Sr_{0.3}Mn_{1-x}M'_xO_3$ (M′ = Al, Ti), J. Appl. Phys. 103 (2008) 043905.
[4] K.A. Gschneidner, V.K. Pecharsky, Magnetocaloric materials, Annu. Rev. Mater Sci. 30 (2000) 387.
[5] J. Lyubina, Magnetocaloric materials for energy efficient cooling, J. Phys. D: Appl. Phys. 50 (2017) 053002.
[6] V. Franco, J.S. Blázquez, J.J. Ipus, J.Y. Law, L.M. Moreno-Ramírez, A. Conde, Magnetocaloric effect: from materials research to refrigeration devices, Progr. Mater. Sci. 93 (2018) 112.
[7] Y.Z. Shao, J.X. Zhang, J.K.L. Lai, C.H. Shek, Magnetic entropy in nanocomposite binary gadolinium alloys, J. Appl. Phys. 80 (1996) 76.
[8] V.K. Pecharsky, K.A. Gschneidner, Gd-Zn alloys as active magnetic regenerator materials for magnetic refrigeration, Cryocoolers 10 (1999) 629.
[9] Z.C. Xu, G.X. Lin, J.C. Chen, A Gd_xHo_{1-x}-based composite and its performance characteristics in a regenerative Ericsson refrigeration cycle, J. Alloys. Comp. 639 (2015) 520.
[10] H. Jagodzinski, H. Fritz, Laves, Obituary. Acta Crystall. A 35 (1979) 343.
[11] M. Balli, D. Fruchart, D. Gignoux, A study of magnetism and magnetocaloric effect in $Ho_{1-x}Tb_xCo_2$ compounds, J. Magn. Magn. Mater. 314 (2007) 16.
[12] F.X. Hu, B.G. Shen, J.R. Sun, Z.H. Cheng, G.H. Rao, X.X. Zhang, Influence of negative lattice expansion and metamagnetic transition on magnetic entropy change in the compound $LaFe_{11.4}Si_{1.6}$, Appl. Phys. Lett. 78 (2001) 3675.
[13] A. Fujita, S. Fujieda, Y. Hasegawa, K. Fukamichi, Itinerant-electron metamagnetic transition and large magnetocaloric effects in $La(Fe_xSi_{1-x})_{13}$ compounds and their hydrides, Phys. Rev. B 67 (2003) 104416.
[14] O. Tegus, E. Brueck, K.H.J. Buschow, F.R. de Boer, Transition-metal-based magnetic refrigerants for room-temperature applications, Nature 415 (2002) 150.
[15] X.Z. Zhou, W. Li, H.P. Kunkel, G. Williams, A criterion for enhancing the giant magnetocaloric effect: (Ni–Mn–Ga) – a promising new system for magnetic refrigeration, J. Phys. Condens. Matter 16 (2004) L39.
[16] W. Tang, W. Lu, X. Luo, B. Wang, X. Zhu, W. Song, Z. Yang, Y. Sun, Particle size effect on $La_{0.}\ 7C_{a0.}3Mn_O3$: size-induced changes of magnetic phase transition order and magnetocaloric study, J. Magn. Magn. Mater. 322 (2010) 2360.
[17] M.H. Phan, S.C. Yu, N.H. Hur, Magnetic and magnetocaloric properties of $(La_{1-x})_{0.8}Ca_{0.2}MnO_3$ (x = 0.05, 0.20) singles crystals, J. Magn. Magn. Mater. 262 (2003) 407.
[18] Z.B. Guo, Y.M. Du, J.S. Zhu, H. Huang, W.P. Ding, D. Feng, Large magnetic entropy change in perovskite-type manganese oxides, Phys. Rev. Lett. 78 (1997) 1142.
[19] P.G. Radaelli, D.E. Cox, M. Marezio, S.W. Cheong, P.E. Schiffer, A.P. Ramirez, Simultaneous structural, magnetic, and electronic transitions in $La_{1-x}Ca_xMnO_3$ with x = 0.25 and 0.50, Phys. Rev. Lett. 75 (1995) 4488.
[20] F. Chen, H.W. Liu, K.F. Wang, H. Yu, S. Dong, X.Y. Chen, X.P. Jiang, Z.F. Ren, J.M. Liu, Synthesis and characterization of $La_{0.825}Sr_{0.175}MnO_3$ nanowires, J. Phys.: Condens. Matter 17 (2005) L467.
[21] P. Katiyar, D. Kumar, T.K. Nath, A.V. Kvit, J. Narayan, S. Chattopadhyay, W.M. Gilmore, S. Coleman, C.B. Lee, J. Sankar, Magnetic properties of self-assembled nanoscale $La_{2/3}Ca_{1/3}MnO_3$ particles in an alumina matrix, Appl. Phys. Lett. 79 (2001) 1327.
[22] R.D. Sánchez, J. Rivas, C. Vazquez-Vazquez, A. Lopez-Quintela, M.T. Causa, M. Tovar, S. Oseroff, Giant magnetoresistance in fine particles of $La_{0.67}Ca_{0.33}MnO_3$ synthesized at low temperatures, Appl. Phys. Lett. 68 (1996) 134.
[23] R. Mahesh, R. Mahendiran, A.K. Raychaudhuri, C.N.R. Rao, Effect of the particle size on the giant mangnetoresistance of $La_{0.67}Ca_{0.33}MnO_3$, Appl. Phys. Lett. 68 (1996) 2291.
[24] A.K.M. Akther Hossain, L.F. Cohen, F. Damay, A. Berenov, J. MacManus-Driscoll, N.McN. Alford, N.D. Mathur, M.G. Blamire, J.E. Evetts, Influence of grain size on magnetoresistance properties of bulk of $La_{0.67}Ca_{0.33}MnO_{3-8}$, J. Magn. Magn. Mater. 192 (1999) 263.
[25] P.K. Siwach, H.K. Singh, O.N. Srivastava, Low field mangenotransport in manganites, J. Phys.: Condens. Matter 20 (2008) 273201.
[26] V. Provenzano, A.J. Shapiro, R.D. Shull, Reduction of hysteresis losses in the magnetic refrigerant $Ga_5Ge_2Si_2$ by the addition of iron, Nature 429 (2004) 853.
[27] P. Nisha, S. Savitha Pillai, Manoj Raama Varma, K.G. Suresh, Critical behavior and mangetocaloric effect in $La_{0.67}Ca_{0.33}Mn_{1-}xCrxO_3$ (x = 0.1, 0.25), Solid State Sci. 14 (2012) 40.
[28] P.T. Phong, L.V. Bau, L.C. Hoan, D.H. Manh, N.X. Phuc, In-Ja Lee, Effect of B-site Ti doping on the magnetic, low–field magnetocaloric and electrical transport

properties of $La_{0.7}Sr_{0.3}Mn_{1-x}Ti_xO_3$ perovskites, J. Alloys Compd. 656 (2016) 920.
[29] A. Selmi, R. M'nassri, W. Cheikhrouhou-Koubaa, N. Chniba Boudjada, A. Cheikhrouhou, Influence of transition metal doping (Fe, Co, Ni and Cr) on magnetic and magnetocaloric properties of $Pr_{0.7}Ca_{0.3}MnO_3$ manganites, Ceram. Int. 41 (2015) 10177.
[30] E. Oumezzine, S. Hcini, El-K. Hlil, E. Dhahri, M. Oumezzine, Effect of Ni-doping on structural, magnetic and magnetocaloric properties of $La_{0.6}Pr_{0.1}Ba_{0.3}Mn_{1-x}NixO_3$ nanocrystalline manganites synthesized by Pechini sol-gel method, J. Alloys Comp. 615 (2014) 553.
[31] Y.D. Zhang, T.L. Phan, T.S. Yang, S.C. Yu, Local structure and magnetocaloric effect for $La_{0.7}Sr_{0.3}Mn_{1-x}Ni_xO_3$, Curr. Appl. Phys. 12 (2012) 803.
[32] S. Raj, H.C. Padhi, P. Raychaudhury, A.K. Nigam, R. Pinto, M. Polasik, F. Pawlowski, D.K. Basa, Valence electronic structure of Mn in undoped and doped lanthanum manganites from relative K-X-ray intensity studies, Nucl. Instr. Meth. Phys. Res. B, 174 2001, p. 344.
[33] A. El-Moez, A. Mohamed, B. Hernando, A.M. Ahmed, Magnetic magnetocaloric and thermoelectric properties of nickel doped manganites, J. Alloys Compd. 692 (2017) 381.
[34] P. Thamilmaran, M. Arunachalam, S. Sankarrajan, K. Sakthipandi, Impact of Ni doping on $La_{0.7}Sr_{0.3}Ni_xMn_{1-x}O_3$ perovskite manganite materials, J. Magn. Magn. Mater. 396 (2015) 181.
[35] P. The-Long Phan, T.D. Zhang, S.C.Yu. Thanh, Crossover from first-order to second-order phase transitions and magnetocaloric effect in $La_{0.7}Ca_{0.3}Mn_{0.91}Ni_{0.09}O_3$, J. Appl. Phys. 115 (2014) 17A912.
[36] C.J. Brinker, G.W. Scherer, Sol-Gel Science, The Physics and Chemistry of Sol-Gel Processing, Academic Press, San Diego, 1990.
[37] A. Gómez, E. Chavarriaga, I. Supelano, C.A. Parra, O. Morán, Evaluation of the magnetocaloric response of nano-sized $La_{0.7}Ca_{0.3}Mn_{1-x}Ni_xO_3$ manganites synthesized by auto-combustion method, AIP Adv. 8 (2018) 056430.
[38] M. Rubinstein, D.J. Gillespie, J.E. Synder, T.M. Tritt, Effect of Gd Co, and Ni doping in La2/3Ca1/3MnO3: resistivity, thermopower, and paramagnetic resonance, Phys. Rev. B 56 (1998) 5412.
[39] A. Gómez, E. Chavarriaga, I. Supelano, C.A. Parra, O. Morán, Tuning the magnetocaloric properties of $La_{0.7}Ca_{0.3}MnO_3$ manganites through Ni-doping, Phys. Lett. A 382 (2018) 911.
[40] L. Damari, J. Pelleg, G. Gorodetsky, Ch. Koren, V. Markovich, A. Shames, X. Wu, D. Mogilyanski, I. Fita, A. Wisniewski, The effect of Ni doping on the magnetic and transport properties in $Pr_{0.5}Ca_{0.5}Mn_{1-x}Ni_xO_3$ manganites, J. Appl. Phys. 106 (2009) 013913.
[41] B. Arun, M.V. Suneesh, M. Vasundhara, Comparative study of magnetic ordering and electrical transport in bulk and nano-grained $Nd_{0.67}Sr_{0.33}MnO_3$ manganites, J. Magn. Magn. Mater. 418 (2016) 265.
[42] M. Sugantha, R.S. Singh, A. Guha, A.K. Raychaudhuri, C.N.R. Rao, Effect of substitution of Mn^3 by other trivalent cations on the colossal magnetoresistance and related properties of the manganates: $La_{0.7}A_{0.3}Mn_{1-x}M_xO_3$ (A = Ca, Sr, Pb; M = Al, Cr, Fe, Co), Mater. Res. Bull. 33 (1998) 1129.
[43] Y.H. Huang, Z.G. Xu, C.H. Yan, Z.M. Wang, T. Zhu, C.S. Liao, S. Gao, G.X. Xu, Soft chemical synthesis and transport properties of $La_{0.7}Sr_{0.3}MnO_3$ granular perovskite, Sol. State Comm. 114 (2000) 43.
[44] S. Vasseur, E. Duguet, J. Portier, G. Goglio, S. Mornet, E. Hadová, K. Knízek, M. Marysko, P. Veverka, E. Pollert, Lanthanum manganese perovskite nanoparticles as possible in vivo mediators for magnetic hyperthermia, J. Magn. Magn. Mater. 302 (2006) 315.
[45] P. Dutta, P. Dey, T. Nath, Effect of nanometric grain size on room temperature magnetoimpedance, magnetoresistance, and magnetic properties of $La_{0.7}Sr_{0.3}MnO_3$, J. Appl. Phys. 102 (2007) 073906.
[46] S.K. Mandal, T.K. Nath, V.V. Rao, Effect of nanometric grain size on electronic-transport, magneto-transport and magnetic properties of $La_{0.7}Ba_{0.3}MnO_3$ nanoparticles, J. Phys. Condens. Matter. 20 (2008) 140.
[47] L. Balcells, J. Fontcuberta, B. Martinez, X. Obradors, High-field magnetoresistance at interfaces in manganese perovskite, Phys. Rev. B 58 (1998) R14697.
[48] P.A. Joy, C. Raj Sankar, S.K. Date, The limiting value of x in the ferromagnetic compositions $La_{1-x}MnO_3$, J. Phys.: Condens. Matter 14 (2002) L663.
[49] B.K. Banerjee, on a generalized approach to first and second order magnetic transitions, Phys. Lett. 12 (1964) 16.
[50] Q.T. The-Long Phan, P.Q. Tran, P.D.H. Thanh, S.C.Yu. Yen, Critical behavior of $La_{0.7}Ca_{0.3}Mn_{1-x}Ni_xO_3$ manganites exhibiting the crossover of first- and second-order phase transitions, Solid State Comm. 184 (2014) 40.
[51] T. Sarkar, A.K. Raychaudhuri, A.K. Bera, S.M. Yusuf, Effect of size reduction on the ferromagnetism of the manganite $La_{1-x}Ca_xMnO_3$ (x = 0.33), New J. Phys. 12 (2010) 123026.
[52] L.E. Hueso, P. Sande, D.R. Miguens, J. Rivas, F. Rivadulla, M.A. Lopez-Quintela, Tuning of the magnetocaloric effect in $La_{0.67}Ca_{0.33}MnO_{3-\delta}$ nanoparticles synthesized by sol-gel techniques, J. Appl. Phys. 91 (2002) 9943.
[53] J.-H. Park, E. Vescovo, H.-J. Kim, C. Kwon, R. Ramesh, T. Venkatesan, Magnetic properties at surface boundary of a half-metallic ferromagnet $La_{0.7}Sr_{0.3}MnO_3$, Phys. Rev. Lett. 81 (1998) 1953.
[54] X. Bohigas, J. Tejada, M.L. Marinez-Sarrion, S. Tripp, R. Black, Magnetic and calorimetric measurements on the magnetocaloric effect in $La_{0.6}Ca_{0.4}MnO_3$, J. Magn. Magn. Mater. 208 (2000) 85.
[55] M.H. Phan, S.C. Yu, Review of the magnetocaloric effect in manganite materials, J. Magn. Magn. Mater. 308 (2007) 325.
[56] C.P. Reshmi, S. Savitha Pillai, K.G. Suresh, Manoj Raama Varma, Room temperature magnetocaloric properties of Ni substituted $La_{0.67}Sr_{0.33}MnO_3$, Solid State Sci. 19 (2013) 130.
[57] N. Kallel, S. Kallel, A. Hagaza, M. Oumezzine, Magnetocaloric properties in the Cr-doped $La_{0.7}Sr_{0.3}MnO_3$ manganites, Phys. B 404 (2009) 285.
[58] S.K. Barik, C. Krishnamoorthi, R. Mahendiran, Effect of Fe substitution on magnetocaloric effect in $La_{0.7}Sr_{0.3}Mn_{1-x}Fe_xO_3$ ($0.05 \le x \le 0.20$), J. Magn. Magn. Mater. 323 (2011) 1015.
[59] P. Zhang, H. Yang, S. Zhang, H. Ge, S. Hua, Magnetic and magnetocaloric properties of perovskite $La_{0.7}Sr_{0.3}Mn_{1-x}Co_xO_3$, Phys. B 410 (2013) 1.
[60] N.S. Bingham, M.H. Phan, H. Srikanth, M.A. Torija, C. Leighton, Magnetocaloric effect and refrigerant capacity in charge-ordered manganites, J. Appl. Phys. 106 (2009) 023909.
[61] P. Lampen, N.S. Bingham, M.H. Phan, H. Kim, M. Osofsky, A. Piqué, T.L. Phan, S.C. Yu, H. Srikanth, Impact of reduced dimensionality on the magnetic and magnetocaloric response of $La_{0.7}Ca_{0.3}MnO_3$, Appl. Phys. Lett. 102 (2013) 062414.
[62] X.X. Zhang, G.H. Wen, F.W. Wang, W.H. Wang, C.H. Yu, G.H. Wu, Magnetic entropy change in Fe-based compound $LaFe_{10.6}Si_{2.4}$, Appl. Phys. Lett. 77 (2000) 3072.
[63] V. Franco, J.S. Blázquez, A. Conde, Influence of Ge addition on the magnetocaloric effect of a Co-containing Nanoperm-type alloy, Appl. Phys. Lett. 103 (2008) 07B316.
[64] V. Franco, J.S. Blázquez, B. Ingale, A. Conde, The magnetocaloric effect and magnetic refrigeration near room temperature: materials and models, Annu. Rev. Mater. Res. 42 (2012) 305.
[65] V.K. Pecharsky Jr., K.A. Gschneidner, Magnetocaloric effect from indirect measurements: magnetization and heat capacity, J. Appl. Phys. 86 (1999) 565.
[66] V. Franco, A. Conde, Scaling laws for the magnetocaloric effect in second order phase transitions: from physics to applications for the characterization of materials, Int. J. Refrig. 33 (2010) 465.
[67] V. Franco, J.S. Blázquez, A. Conde, Field dependence of the magnetocaloric effect in materials with a second order phase transition: a master curve for the magnetic entropy change, Appl. Phys. Lett. 89 (2006) 222512.
[68] H. Oesterreicher, F.T. Parker, Magnetic cooling near Curie temperatures above 300 K, J. Appl. Phys. 55 (1984) 4334.
[69] V. Franco, J.S. Blázquez, A. Conde, The influence of Co addition on the magnetocaloric effect of Nanoperm-type amorphous alloys, Appl. Phys. Lett. 100 (2006) 064307.
[70] Y.S. Reddy, P. Kistaiah, C.V. Reddy, Elastic properties of double layered manganites $R_{1.2}Sr_{1.8}Mn_2O_7$ (R = La, Pr, Nd, Sm), Rare Met. 33 (2014) 166.
[71] A. Asamitsu, Y. Moritomo, R. Kumai, Y. Tomioka, Y. Tokura, Magnetostructural phase transitions in $La_{1-x}Sr_xMnO_3$ with controlled carrier density, Phys. Rev. B 54 (1996) 1716.
[72] C.M. Xiong, J.R. Sun, Y.F. Chen, B.G. Shen, J. Du, Y.X. Li, Relation between magnetic entropy and resistivity in $La_{0.67}Ca_{0.33}MnO_3$, J IEEE Trans. Magn. 41 (2005) 122.
[73] H.L. Ju, C. Kwon, Q. Li, R.L. Greene, T. Venkatesan, Giant magnetoresistance in $La_{1-x}Sr_xMnO_z$ films near room temperature, Appl. Phys. Lett. 65 (1994) 2108.
[74] S. Jin, T.H. Tiefel, M. McCormack, R.A. Fastnacht, R. Ramesh, L.H. Chen, Thousand fold change in resistivity in magnetoresistive La-Ca-Mn-O films, Science 264 (1994) 413.
[75] N. Kallel, G. Dezanneau, J. Dhahri, M. Oumezzine, H. Vincent, Structure magnetic and electrical behaviour of $La_{0.7}Sr_{0.3}Mn_{1-x}Ti_xO_3$ with $0 \leqslant x \leqslant 0.3$, J. Magn. Magn. Mater. 261 (2003) 56.
[76] L. Righi, P. Gorria, M. Insausti, J. Gutiérrez, J.M. Barandiaran, Influence of Fe in giant magnetoresistance ratio and magnetic properties of $La_{0.7}Ca_{0.3}Mn_{1-x}Fe_xO_3$ perovskite type compounds, J. Appl. Phys. 81 (1997) 5767.
[77] I.O. Troyanchuk, N.V. Samsonenko, A. Nabiaiek, H. Szymczak, Magnetic interactions and phase transitions in the Co- and Ni-doped manganites, J. Magn. Magn. Mater. 168 (1997) 309.
[78] S. Pal, E. Bose, B.K. Chaudhuri, H.D. Yang, S. Neeleshwar, Y.Y. Chen, Effect of Ni doping in rare-earth manganite $La_{0.7}Pb_{0.3}Mn_{1-x}Ni_xO_3$ (x = 0.0-0.5), J. Magn. Magn. Mater. 293 (2005) 872.
[79] H. Terashita, J. Neumeier, Bulk magnetic properties of $La_{1-x}Ca_xMnO_3$ ($0 \leqslant x \leqslant 0.14$): signatures of local ferromagnetic order, J. Phys. Rev. B 71 (2005) 134402.
[80] H.Y. Hwang, T.T.M. Palstra, S.W. Cheong, B. Batlogg, Pressure effects on the magnetoresistance in doped manganese perovskites, Phys. Rev. B 52 (1995) 15046.
[81] B. Roy, A. Poddar, S. Das, Electrical transport properties and magnetic cluster glass behavior of $Nd_{0.7}Sr_{0.3}MnO_3$ nanoparticles, J. Appl. Phys. 100 (2006) 104318.
[82] G.J. Snyder, R. Hiskes, S. DiCarolis, M.R. Beasley, T.H. Geballe, Phys. Rev. B 53 (1996) 14434.
[83] L.I. Balcells, A.E. Carrillo, B. Martinez, J. Fontcuberta, Enhanced field sensitivity close to the percolation in magneto resistive $La_{2/3}Sr_{1/3}MnO_3/CeO_2$ composites, Appl. Phys. Lett. 74 (1999) 4014.
[84] K. Kubo, N. Ohata, A quantum theory of double exchange, J. Phys. Soc. Jpn. 33 (1992) 21.
[85] D. Worledge, L. Mieville, T. Geballe, On-site Coulomb repulsion in the small polaron system $La_{1-x}Ca_xMnO3$, Phys. Rev. B 57 (1998) 15267.
[86] A.M. Ahmed, A. El-Moez, A. Mohamed, M.A. Abdellateef, H.A. El-Ghanny, Magnetoresistive properties of Ni-doped $La_{0.7}Sr_{0.3}MnO_3$ manganites, Rare Met. 35 (2016) 551.
[87] I.G. Austin, N.F. Mott, Polarons in crystalline and non-crystalline materials, Adv. Phys. 18 (1969) 41.
[88] A. Banergee, S. Bhattacharya, B.K. Chaudhuri, J. Appl. Phys. 91 (2002) 5125.
[89] G. Venkataiah, Y. Kalyana Lakshmi, V. Prasad, P. Venugopa Reddy, Influence of particle size on electrical transport properties of $La_{0.67}Sr_{0.33}MnO_3$ manganite system, J. Nanosci. Nanotechnol. 7 (2007) 1.
[90] A.P. Ramirez, Colossal magnetoresistance, J. Phys. Condensed Matter. 9 (1997) 8171.
[91] H.Y. Hwang, S.W. Cheong, N.P. Ong, B. Batlogg, Spin-polarized intergrain tunneling in $La_{2/3}Sr_1/3MnO_3$, Phys. Rev. Lett. 77 (1996) 2041.

[92] D.H. Manh, P.T. Phong, T.D. Thanh, L.V. Hong, N.X. Phuc, Low-field magnetoresistance of $La_{0.7}Ca_{0.3}MnO_3$ perovskite synthesized by reactive milling method, J. Alloys Compd. 499 (2010) 131.
[93] J. Rivas, L.E. Hueso, A. Fondado, F. Rivadulla, M.A. Lopez-Quintela, Low field magnetoresistance effects in fine particles of $La_{0.67}Ca_{0.33}MnO_3$ perovskites, J. Magn. Magn. Mater. 221 (2000) 57.
[94] K. Navin, R. Kurchania, Structural magnetic and transport properties of the $La_{0.7}Sr_{0.3}MnO_3$-ZnO nanocomposites, J. Magn. Magn. Mater. 448 (2018) 228.
[95] J. Khelifi, E. Dhahri, E.K. Hlil, Correlation between electrical, magnetocaloric properties and critical behavior in $(La_{0.75}Nd_{0.25})_{2/3}(Ca_{0.8}Sr_{0.2})_{1/3}MnO_3$, Solid State Comm. 249 (2017) 19.
[96] C.M. Xiong, J.R. Sun, Y.F. Chen, B.G. Shen, J. Du, Y.X. Li, Relation between magnetic entropy and resistivity in $La_{0.67}Ca_{0.33}MnO_3$, IEEE Trans. Magn. 41 (2005) 122.
[97] A.J. Millis, P.B. Littlewood, B.I. Shraiman, Double exchange alone does not explain the resistivity of $La_{1-x}Sr_xMnO_3$, Phys. Rev. Lett. 74 (1995) 5144.